

Dalton Transactions

An international journal of inorganic chemistry

Accepted Manuscript

This article can be cited before page numbers have been issued, to do this please use: A. Paul, K. Das, A. Karmakar, M. F. C. Guedes da Silva and A. J. L. Pombeiro, *Dalton Trans.*, 2020, DOI: 10.1039/D0DT02172E.



This is an Accepted Manuscript, which has been through the Royal Society of Chemistry peer review process and has been accepted for publication.

Accepted Manuscripts are published online shortly after acceptance, before technical editing, formatting and proof reading. Using this free service, authors can make their results available to the community, in citable form, before we publish the edited article. We will replace this Accepted Manuscript with the edited and formatted Advance Article as soon as it is available.

You can find more information about Accepted Manuscripts in the [Information for Authors](#).

Please note that technical editing may introduce minor changes to the text and/or graphics, which may alter content. The journal's standard [Terms & Conditions](#) and the [Ethical guidelines](#) still apply. In no event shall the Royal Society of Chemistry be held responsible for any errors or omissions in this Accepted Manuscript or any consequences arising from the use of any information it contains.

A mechanistic insight into the rapid and selective removal of Congo Red by an amide functionalised Zn(II) Metal Organic Framework

Anup Paul,^{*,†} Kabita Das,[‡] Anirban Karmakar,[†] M. Fátima C. Guedes da Silva,[†] Armando J. L. Pombeiro^{*,†}

[†]*Centro de Química Estrutura, Instituto Superior Técnico, Universidade de Lisboa, Av. Rovisco Pais, 1049-001 Lisboa. Portugal.*

[‡]*Department of Environmental Studies, North-Eastern Hill University, Meghalaya, Shillong 793022, India*

Abstract:

The new CPs [Zn(μ -1 κ OO':2 κ N-L)(H₂O)(BDC)_{0.5}]_n.n(DMF) (**1**), [Cd(μ -1 κ O:2 κ N-L)₂(H₂O)₂]_n (**2**) and [Pb(μ -1 κ OO':2 κ O'-L)(μ -1 κ O:2 κ O':3 κ N-L)]_n (**3**) [L = 4-(pyridin-3-ylcarbamoyl)benzoate; BDC = benzene-1,4-dicarboxylate] were synthesized and characterized by elemental, FT-IR, powder and single-crystal X-ray diffraction analyses. Single crystal X-ray diffraction analysis discloses 1D polymeric architectures for **1** and **2** and a 2D one for **3**. The topological analysis exemplifies a 2,2,3-connected 3-nodal net with the point symbol {8².12}₂{8}₃ for **1**, a 2,4-connected bimodal net for **2** and a 3,4,7-connected trinodal net for **3**. The CP **1** exhibits a selective removal of Congo Red (CR) dye amongst various dyes. It can be recycled and reused without any significant loss of its dye removal efficiency. An insight in the selective removal of the Congo dye is provided by *in silico* studies, being accounted for by anion- π , cation- π and π - π stacking interactions, involving the Zn(II) ion, phenyl rings and O_{carboxylate} of **L**, and phenyl, naphthalene rings and O_{sulfonate} of CR.

***Corresponding authors**, E-mail: kanupual@gmail.com, pombeiro@tecnico.ulisboa.pt.

Introduction

Organic dyes, as important industrial components in paper, textiles, plastics, rubber and coatings etc. are extensively used.¹ Under an environmental perspective, the removal of these harmful dyes before being released into the natural system is an important matter.¹ A lot of methods for the elimination of dyes from an aqueous environment have been developed, namely by using activated carbon, filtration, photocatalysis, adsorption, and so on.²⁻⁹ However, some of the methods, such as using activated carbon and filtration, are merely effective for removal of low concentrations of pollutants from water. The adsorption method in particular with no chemical deterioration is considered to be highly advantageous due to its effectiveness, efficiency and economy. However, a major setback associated with these adsorbents concerns their reusability. It is thus necessary to develop a kind of material to overcome these difficulties, which will not only reduce the pollution caused by the dyes but will also achieve a high selectivity, being able to be recycled.

Over the years, a great attention has been paid on the ever-increasing research area of novel functional metal-organic frameworks (MOFs) or coordination polymers (CPs) due to their attractive features, such as luminescence, magnetism, applications in catalysis, etc.¹⁰⁻¹⁶ A key to building an ideal MOF is usually lying in the design of appropriate ligands and generally a simple adjustment in the ligand framework can result in novel structures.^{10,11,16} Apart from a wide range of applications of MOFs in various fields, they have also been utilized as an excellent material for adsorption of dyes.⁶⁻⁹ However, the majority of MOFs that possess this feature has high dimensional structures.¹⁷⁻²⁰ On the contrary, MOFs with low-dimensional structures exhibiting a high dye adsorption are rare, but this ability can be fostered by promoting specific interactions, such as electrostatic connections, hydrogen-bonding and π - π interaction.¹⁷ These

specific interactions between MOFs or CPs and dye endow the former the ability to discriminate different types of dyes towards a selective separation. The design and synthesis of new low dimensional MOFs that can lead to the separation of dyes effectively is thus an important issue.

Pyridyl-amide functionalized ligands are known to behave as good linkers for generating multi-dimensional MOFs that have been used in a number of applications, such as, in gas storage and separation, optical sensing, catalysis, as well as for adsorption of dyes.^{13,15,16,21–25} We have already reported some CPs, based on new amide functionalized ligands, which were found to be effective heterogeneous catalysts in various organic transformations.^{13,16,26} Such a kind of ligands has two advantages: (i) the ligand comprises multiple coordinating groups suitable for building extended frameworks with a large surface area, and (b) the amide groups are both hydrogen-bonding donors and acceptors, having the possibility to establish interactions with the targeted dyes.

In this context, we synthesized a new ligand source (Fig. 1), by incorporating the pyridyl N-nitrogen at the *meta* position instead of at *para* position which was the case in the previously reported analogous one.¹³ Although a search in the CSD database found a report on this ligand by Feng et al.²⁷ generated *in situ* for the construction of MOFs and its direct synthesis and isolation has been recently reported by us but not the detailed synthesis protocol.²⁸ Herein, we describe the detailed syntheses and characterization of 4-(pyridin-3-ylcarbamoyl)benzoic acid (**HL**) and of its derived CPs $[\text{Zn}(\mu\text{-}1\kappa\text{OO}':2\kappa\text{N-L})(\text{H}_2\text{O})(\text{BDC})_{0.5}]_n \cdot n(\text{DMF})$ (**1**), $[\text{Cd}(\mu\text{-}1\kappa\text{O}:2\kappa\text{N-L})_2(\text{H}_2\text{O})_2]_n$ (**2**) and $[\text{Pb}(\mu\text{-}1\kappa\text{OO}':2\kappa\text{O}'\text{-L})(\mu\text{-}1\kappa\text{O}:2\kappa\text{O}':3\kappa\text{N-L})]_n$ (**3**). CP **1** was found to possess an excellent removal ability of Congo Red dye over other dyes. A theoretical study is also presented in order to get a mechanistic insight of this adsorption process.

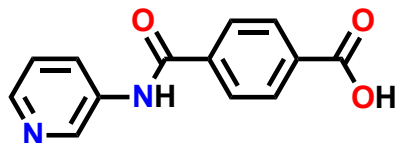


Fig. 1. 4-(pyridin-3-ylcarbamoyl)benzoic acid (**HL**).

Experimental Section

Materials and methods

Solvents used in the reactions were dried and distilled prior to their use.²⁹ Benzene-1,4-dicarboxylic acid (BDCA), 3-aminopyridine, thionyl chloride (SOCl₂) and the metal nitrates Zn(NO)₃·6H₂O (98.0% purity) were purchased from Sigma Aldrich Chemical Co. and used as such. FT-IR spectra were recorded on a Bruker Vertex 70 instrument in KBr pellets. ¹H (300 MHz) and ¹³C (75.45 MHz) NMR spectra were obtained at room temperature (RT) on a Bruker Avance II + 300 (UltraShieldTMMagnet) spectrometer using tetramethylsilane [Si(CH₃)₄] as an internal reference. Carbon, hydrogen and nitrogen elemental analyses were carried out by the Microanalytical Service of the Instituto Superior Técnico. Nitrogen adsorption isotherm was collected on a Micromeritics ASAP 2060 gas sorption instrument at 77 K; the sample was pre-treated in a vacuum oven at 150 °C for 12 h before analysis. Single crystal X-ray diffraction data were collected using a Bruker APEX-II PHOTON 100 diffractometer with graphite monochromated Mo-Kα (λ = 0.71069) radiation. Powder X-ray diffraction (PXRD) was conducted in a D8 Advance Bruker AXS (Bragg Brentano geometry) θ-2θ diffractometer, with copper radiation (Cu Kα, λ = 1.5406 Å) and a secondary monochromator, operated at 40 kV and 40 mA. Flat plate configuration was used, and the typical data collection range was between 5° and 40°. Thermal properties were analyzed with a Perkin-Elmer Instrument system (STA6000)

at a heating rate of 10 °C min⁻¹ under a dinitrogen atmosphere. Electronic absorption and solid-state emission spectra at room temperature were recorded on Perkin-Elmer LAMBDA 750 UV-visible spectrophotometer and Perkin Elmer Fluorescence Spectrometer (LS-55), respectively. Electrospray ionization mass spectrometric data (ESI-MS) were acquired in DMSO on a Bruker Micro TOF QII, and THERMO Finnigan LCQ Advantage Max ion trap Mass Spectrometer.

Synthesis and characterization

Synthesis of 4-(pyridin-3-ylcarbamoyl)benzoic acid (HL)

The pro-ligand **HL** was synthesized in two steps. In the first step its ester form **MeL** was synthesized according to a modified procedure reported earlier¹³, where terephthalic acid monomethyl ester chloride (1.98 g, 10.0 mmol) in 20 mL THF was added dropwise to a mixture of 3-aminopyridine (0.94 g, 10.0 mmol) in 20 mL THF and 3 mL triethylamine at 0°C, and was stirred for 24 h. The white suspension thus formed was filtered off and washed with 2 mL of water and dried. The crude product was recrystallized using CH₂Cl₂ to obtain the pure product (**MeL**). Yield: 2.10 g (72%). ¹H NMR (DMSO-*d*₆, δ ppm) 10.97 (1H, s, NH), 8.42 (1H, d, H-py), 8.19 (1H, d, H-py), 8.10 (4H, dd, H-bz), 7.89 (1H, t, H-py), 7.15 (1H, t, H-py), 3.93 (3H, s, OCH₃). Anal. Calcd. for C₁₄H₁₂O₃N₂: C, 65.62; H, 4.72; N, 10.93%. Found: C, 65.66; H, 4.80; N, 10.89%. FT-IR (cm⁻¹): 3236(m), 3190(m), 3111(m), 3050(m), 1718(s), 1671(s), 1593(m), 1579(s), 1541(s), 1507(m), 440(s), 1310(s), 1287(s), 1240(m), 1111(s), 784(m), 714(m).

In the second step, **MeL** was hydrolyzed according to a reported procedure³⁴ to obtain the pro-ligand **HL**. Yield: 1.6g (76%). The relevant ¹H and ¹³C-NMR spectra (¹H and ¹³C-NMR) are given in Figs. S1-S2, ESI. Anal. Calcd for C₁₃H₁₀N₂O₃: C, 64.46; H, 4.16; N, 11.56. Found: C, 64.63; H, 4.23; N, 11.61. FT-IR (KBr, cm⁻¹): 3279 (bs), 1703 (w), 1643 (s), 1522 (s), 1406(w),

1274 (br), 1181 (w) 1103 (w), 1010 (w), 865 (w), 790 (s), 700 (br), 641 (w). $^1\text{H-NMR}$ (300 MHz, $\text{DMSO-}d_6$, δ ppm): δ 13.21 (s, 1H, COOH), 10.66 (s, 1H, NH), 8.94 (s, 1H, H_{py}), 8.33 (d, 1H, $J = 6.0$ Hz, H_{py}), 8.20 (d, 1H, $J = 6.0$ Hz, H_{py}), 8.06 (s, 4H, Ar-H), 7.44 (t, 1H, H_{py}). $^{13}\text{C-NMR}$ (77 MHz, $\text{DMSO-}d_6$, δ ppm): 167.17, 165.71, 145.26, 142.47, 138.52, 136.08, 134.02, 129.82, 128.46, 127.88, 124.04. ESI-MS : m/z $[(\text{M} + \text{H})]^+$, Calcd. 243.07, found 243.11, $[(\text{M} + \text{Na})]^+$, Calcd. 265.07, found 264.91.

Synthesis of $[\text{Zn}(\mu\text{-}1\kappa\text{OO}'\text{:}2\kappa\text{N-L})(\text{H}_2\text{O})(1,4\text{-BDC})_{0.5}]_n \cdot n(\text{DMF})$ (**1**)

A mixture of **HL** (15 mg, 0.067 mmol), $\text{Zn}(\text{NO}_3)_2 \cdot 6\text{H}_2\text{O}$ (10 mg, 0.060 mmol) and benzene-1,4-dicarboxylic acid (BDCA) (10 mg, 0.060 mmol) in DMF: H_2O (1:1, v/v) in a sealed 8 mL glass vessel was heated at 75 °C for 28 h. White crystals of **1** deposited at the glass vial, were separated by filtration and washed with deionized water, DMF and then dried in air. Yield: 60%. Anal. Calcd for $\text{C}_{20}\text{H}_{20}\text{N}_3\text{O}_7\text{Zn}$: C, 50.07; H, 4.20; N, 8.76. Found: C, 49.98; H, 4.23; N, 8.74. IR (KBr/pellet, cm^{-1}): 3322 (br), 1648 (s), 1593 (m), 1531 (s), 1482 (m), 1330 (w), 1295 (w), 1142 (w), 1019 (w), 799 (m), 736 (m), 642 (m).

Synthesis of $[\text{Cd}(\mu\text{-}1\kappa\text{O}:2\kappa\text{N-L})_2(\text{H}_2\text{O})_2]_n$ (**2**)

A similar synthetic procedure as that used for **1** was followed, but using **HL** (15 mg, 0.067 mmol) and $\text{Cd}(\text{NO}_3)_2 \cdot 4\text{H}_2\text{O}$ (10 mg, 0.060 mmol) in DMF: H_2O (1 mL:1 mL). White crystals of **2** suitable for X-ray diffraction analysis obtained were obtained, removed by filtration and subsequently washed with water, DMF and dried in air. Yield: 68%. Anal. Calcd for $\text{C}_{26}\text{H}_{22}\text{CdN}_4\text{O}_8$: C, 49.50; H, 3.51; N, 8.88. Found: C, 49.55; H, 3.53; N, 8.90. IR (KBr/pellet, cm^{-1}): 3272 (br), 1669 (s), 1538 (s), 1482 (s), 1427 (w), 1385 (s), 1312 (s), 1286 (m), 1193 (w), 1109 (m), 1020 (w), 945 (w), 872 (w), 805 (s), 741 (s), 644 (s), 626 (m).

Synthesis of $[\text{Pb}(\mu\text{-}1\kappa\text{OO}':2\kappa\text{O}'\text{-L})(\mu\text{-}1\kappa\text{O}:2\kappa\text{O}':3\kappa\text{N-L})]_n$ (**3**)

A similar synthetic procedure as that used for **1** was followed, but using **HL** (15 mg, 0.067 mmol) and $\text{Pb}(\text{NO}_3)_2$ (10 mg, 0.060 mmol) in DMF:H₂O (1 mL:1 mL). The white crystals of **3** suitable for X-ray diffraction analysis were filtered off and subsequently washed with water, DMF and dried in air. Yield: 70%. Anal. Calcd for $\text{C}_{26}\text{H}_{18}\text{N}_4\text{O}_6\text{Pb}$: C, 45.28; H, 2.63; N, 8.12. Found: C, 45.25; H, 2.66; N, 8.10. IR (KBr/pellet, cm^{-1}): 3301 (br), 1648 (m), 1586 (m), 1538 (s), 1481 (w), 1330 (m), 1296 (w), 1184 (w), 1048 (w), 1018 (w), 795 (w), 715 (w), 700 (w).

Crystal structure determination

X-ray quality single crystals of the compounds **1-3** were immersed in cryo-oil, mounted in a nylon loop and measured at room temperature. Intensity data were collected using a Bruker APEX-II PHOTON 100 diffractometer with graphite monochromated Mo-K α (λ 0.71069) radiation. Data were collected using phi and omega scans of 0.5° per frame and a full sphere of data was obtained. Cell parameters were retrieved using Bruker SMART³⁰ software and refined using Bruker SAINT³⁰ on all the observed reflections. Absorption corrections were applied using SADABS.³¹ Structures were solved by direct methods by using the SHELXS-2014 package³² and refined with SHELXL-2014/6.³² Calculations were performed using the WinGX System-Version 2014.1.³³ The hydrogen atoms attached to carbon and nitrogen atoms were inserted at geometrically calculated positions and included in the refinement using the riding-model approximation; $U_{\text{iso}}(\text{H})$ were defined as 1.2 U_{eq} of the parent atoms for phenyl and 1.5 U_{eq} of the parent atoms for the methyl groups and nitrogen atoms. Least square refinements with anisotropic thermal motion parameters for all the non-hydrogen atoms and isotropic ones for the remaining atoms were employed. Crystallographic data are summarized in Table 1 and selected

bond distances and angles are presented in Table S1-S2 (Supplementary Information file). CCDC 2010625-2010627 contains the supplementary crystallographic data for this paper. These data can be obtained free of charge from The Cambridge Crystallographic Data Centre via www.ccdc.cam.ac.uk/data_request/cif.

In silico Studies

Molecular docking was done using HEX 8.0.0 software and visualization was performed using Discovery Studio 3.5 software. The parameters used for docking include correlation type shape only, FFT mode 3D, grid dimension 0.6, receptor range 180, ligand range 180, twist range 360, distance range 40.

Determination of point of zero charge (pH_{pzc})

For zero point charge determination (pH_{pzc}) the pH drift method was used.^{34,35} 20 mL solutions were prepared at different pH (4-12) in distilled water using HCl and NaOH, whereafter 30 mg of **1** were then added to each solution. The flasks were then kept for 24 h and the final pH of the solutions were measured. The pH_{pzc} of **1** was determined by plotting the final pH versus the initial one. The pH measurement was carried out using an HANNA HI 2211 pH meter.

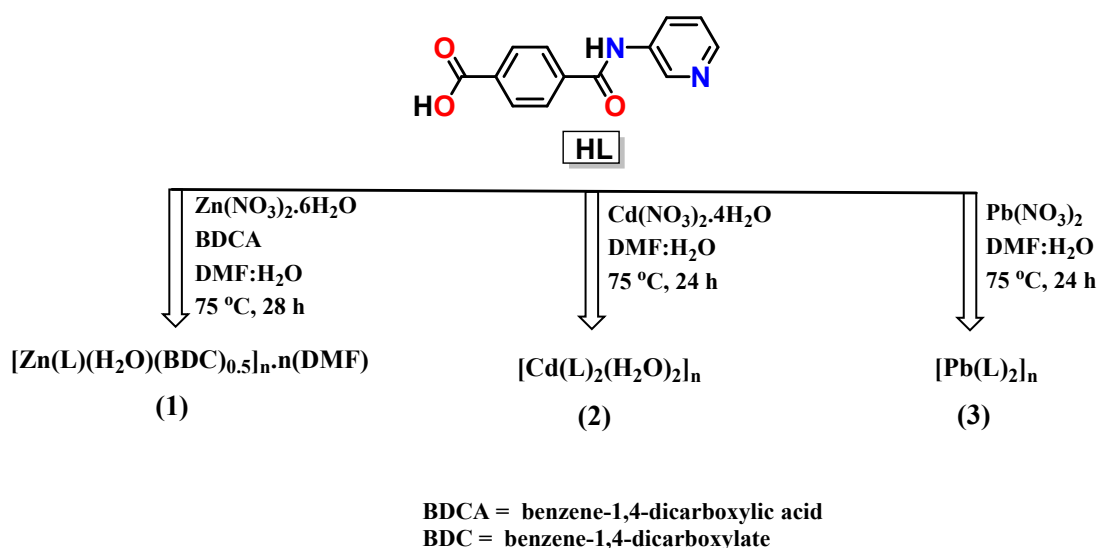
Results and Discussion

Syntheses and Characterisation

The pro-ligand 4-(pyridin-3-ylcarbamoyl)benzoic acid (**HL**) was synthesized by reacting 3-aminopyridine with methyl 4-(chlorocarbonyl)benzoate in anhydrous THF in the presence of triethylamine, followed by hydrolysis according to a procedure reported earlier.²⁸ The coordination polymers **1-3** were synthesized by the hydrothermal reaction of **HL** with

Zn(NO₃)₂·6H₂O [in the presence of benzene-1,4-dicarboxylic acid (BDCA)], Cd(NO₃)₂·4H₂O or Pb(NO₃)₂, respectively (Scheme 1).

The pro-ligand **HL** was characterized by elemental analyses, IR and multinuclear (¹H and ¹³C) NMR techniques, whereas the CPs **1-3** were characterized by elemental analysis, IR and thermogravimetric analyses. Furthermore, the structural features of the CPs **1-3** were unequivocally obtained by single-crystal X-ray diffraction analysis (discussed below). In the ¹H NMR spectrum, **HL** displays characteristic resonances due to the –COOH and –NH protons at δ 13.30 and 10.63, respectively (Fig. S1). The phenyl ring protons resonate in the range of δ 8.94–7.44. In its ¹³C NMR spectrum, the signal due to –COOH appears at δ 166.25, along with other resonances at their usual positions (Fig. S2). The FT-IR spectrum of the pro-ligand **HL** displays a sharp and strong band at 1705 cm⁻¹ attributable to [ν(OCO)] stretching vibrations which upon coordination to the metal centre shifts to a lower frequency at ca. 1648 cm⁻¹, suggesting, in **1-3**, the coordination of the deprotonated carboxylic acid group (Fig. S3). To corroborate that the crystal structures of **1-3** are representative of the synthesized bulk materials, powder-XRD was also carried out. The experimental and simulated powder-XRD patterns of **1-3** clearly demonstrate that the synthesized bulk materials are of a similar nature (Figs. S4-S6).



Scheme 1. Syntheses of CPs 1-3.

Crystal Structure Analysis of 1-3

Single-crystal X-ray diffraction studies of $[\text{Zn}(\mu\text{-}1\kappa\text{OO}':2\kappa\text{N-L})(\text{H}_2\text{O})(\text{BDC})_{0.5}]_n \cdot n(\text{DMF})$ (**1**) reveal that it crystallizes in the triclinic P-1 space group, and that the asymmetric unit contains one Zn^{2+} ion, one L^- ligand, half benzenedicarboxylate, one water ligand and one non-coordinated DMF molecule (Figs. 2a-b). A rhombic grid type one-dimensional double chain framework having approximately $8 \times 14 \text{ \AA}^2$ channels is observed along the crystallographic c -axis (Fig. 2c; potential accessible void of 45.7 \AA^3 per unit cell). Since the Zn-O bonds are well below the sum of the Van der Waals radii (1.39 and 1.52 Å, respectively; see below and Table S1 for selected bond distances and angles), the Zn(II) centre shows a distorted octahedral geometry with three coordination sites being occupied by the chelating $\text{O}_{\text{carboxylate}}$ atoms and the $\text{N}_{\text{pyridine}}$ from two L^- ligands, other two filled by the chelating $\text{O}_{\text{carboxylate}}$ atoms of BDC and the remaining position being occupied by a water molecule. In this way each metal centre is linked to two different L^- ligands whereas each L^- ligand connects two different metal ions.

Fig. 2. (a) The molecular structure of framework **1** with partial atom labelling scheme. (b) One dimensional double chain structure of framework **1** (DMF molecules are represented as space filling model). (c) Hydrogen bonded network of **1**.

The Zn–O bond lengths are in the range of 2.006(3)-2.521(3) Å and the Zn–N length is 2.064(3) Å. The Zn···Zn distance between the two-symmetry related metal centres crosswise the benzoate or the L moieties are of 10.853(4) or 14.018(4) Å, respectively. The DMF molecules are encapsulated into the lattice via hydrogen bonding interactions involving the water ligands as donors [O5-H5B···O7, D···A 2.646(5) Å, <DHA 172°]. Additional N-H···O and O-H···O interactions are also significant which help to expand and stabilize the framework to the third dimension (Table S2, supporting information). Intense $\pi\cdots\pi$ interaction between vicinal phenyl and (slightly offset) pyridine rings were detected (*centroid···centroid* distances of 3.699 Å).

We have obtained another interesting one-dimensional double chain framework, [Cd(μ -1 κ O:2 κ N-L)₂(H₂O)₂]_n (**2**) upon performing the reaction of 4-(pyridin-3-ylcarbamoyl)benzoic acid (**HL**) with cadmium(II) nitrate in a dimethylformamide-water solvent mixture. The asymmetric unit of **2** contains one deprotonated L⁻ ligand, one Cd²⁺ ion and one water molecule. Upon symmetry expansion a polymeric structure is revealed (Fig. 3a) where the Cd centre presents an octahedral coordination environment made of two O_{carboxylate} atoms from two L⁻ units [Cd1-O1, 2.2900(12) Å], two N_{pyridyl} atoms from other two [Cd1-N2, 2.3139(13) Å] and two water molecules [Cd1-O4, 2.3425(13) Å] (Fig. 3b). In this framework, the organic ligand is twisted as shown by the dihedral angle of 58.06° between the phenyl and the pyridyl rings, and the C5-C8-N1-C9 torsional angle of 178.71°. A rhombic grid type one-dimensional double chain framework is observed having approximately 4 x 8 Å² channels along the crystallographic *a*-

axis (Fig. 3b). Strong $\pi\cdots\pi$ interactions could also be detected in **2** with almost perfect dipole-dipole stacks of vicinal pyridine moieties (*centroid* \cdots *centroid* distances of 3.456 Å).

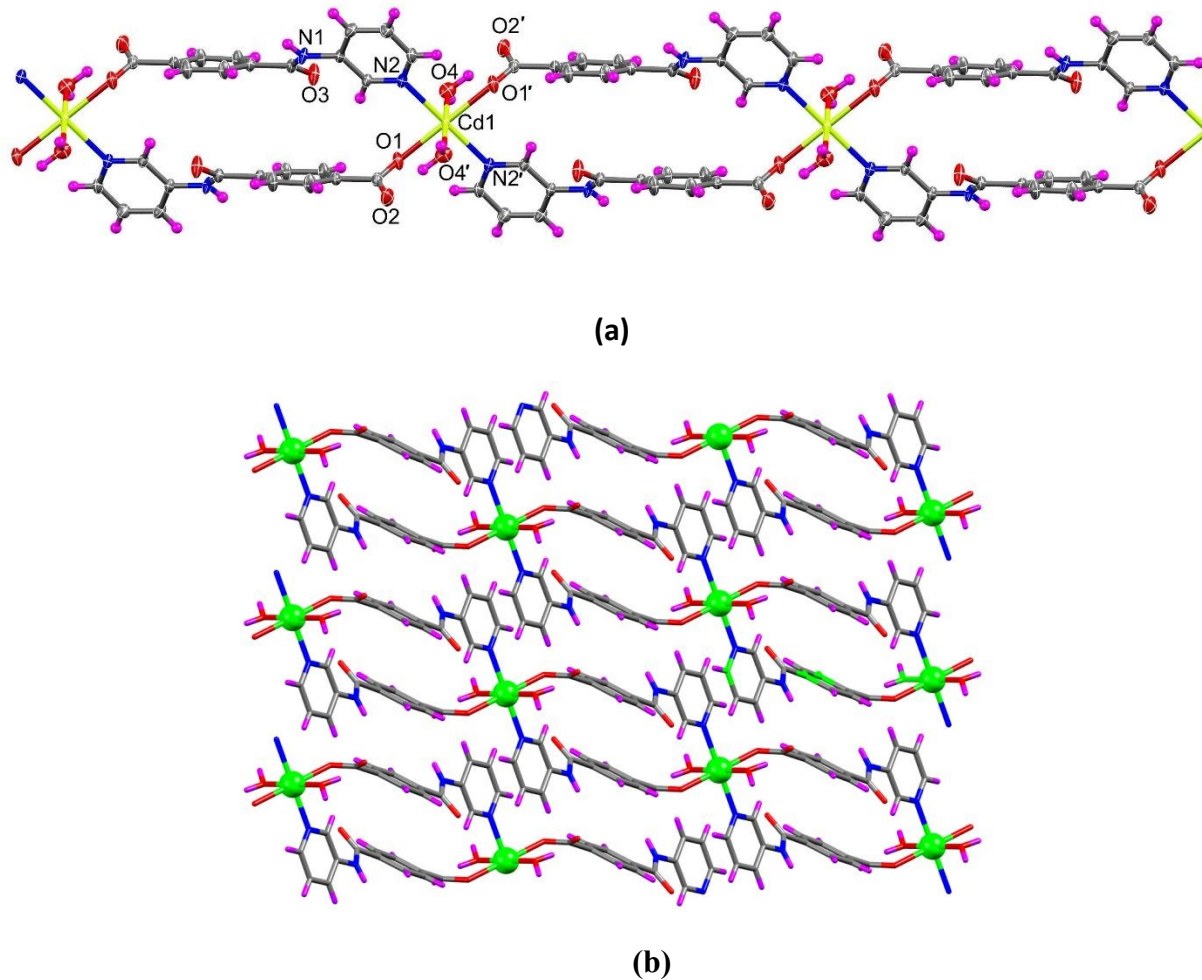
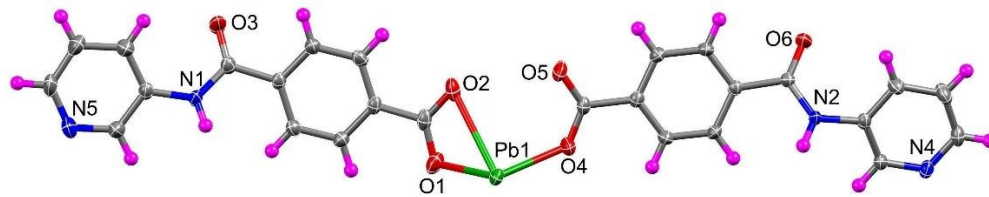


Fig. 3. (a) 1D double chain structure of framework **2**. (b) Packing view of compound **2**.

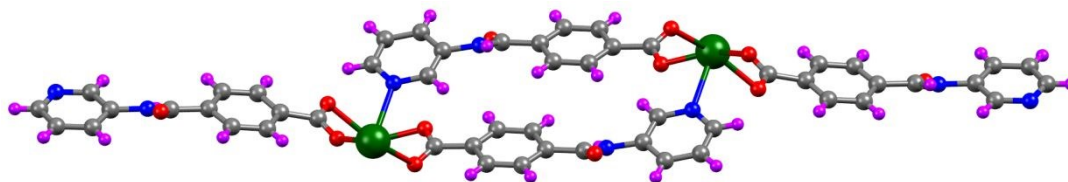
The water ligands in **2** simultaneously donate to the non-coordinated $O_{\text{carboxylate}}$ of L^- and to the O_{keto} atom in a vicinal chain [O4-H4A \cdots O2: D \cdots A 2.6919(19) Å, \angle DHA 164°; O4-H4B \cdots O3:

D \cdots A 2.7546(19) Å, <DHA 171°] therefore expanding the structure to the second and then to the third dimension.

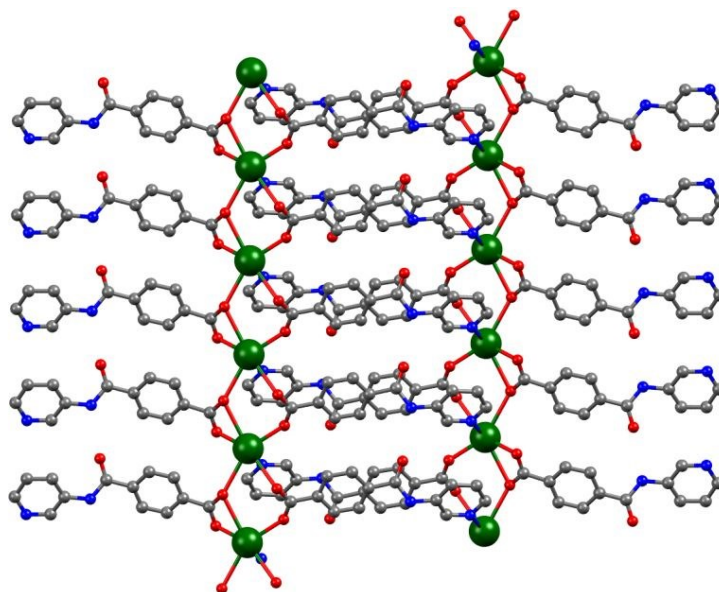
The single-crystal X-ray diffraction analysis disclosed that asymmetric unit of **3** contains one Pb(II) cation and two deprotonated L⁻ ligands expanding, by symmetry, to the 2D CP [[Pb(μ -1 κ OO':2 κ O'-L)(μ -1 κ O:2 κ O':3 κ N-L)]_n (**3**). The Pb(II) centre presents an hexa-coordinate environment constructed with the O_{carboxylate}-atoms from four L⁻ ligands, one of those acting as a bridging chelate donor, the remaining binding position being engaged with the N_{pyridyl} atom from a fifth L⁻ moiety (Figs. 4a-c). The Pb–O bond lengths assume values between 2.3817(17) and 2.925(2) Å (Table S3) and the Pb–N4 distance is 2.534(2) Å. The distance between the Pb(II) cations in the {PbOCO}₂ bimetallic ring is 5.1144(3) Å, and of 13.360(1) Å when going through the L skeletons, in {Pb(L)}₂. There are two different types of L⁻ ligands in the structure of **3**: one in which this anion coordinates to three different Pb(II) cations through a bridging O_{carboxylate}- and the N_{pyridyl}- atoms, hence occupying internal positions in the structure, and another where it is coordinated to two different metal centres by means of bridge-chelating O_{carboxylate} groups. The organic moieties are not planar, the dihedral angles between the phenyl and the pyridyl rings assuming values of 8.91° and 13.51° depending on the ligand being coordinated to two or to three metal cations; additionally, and in the same order, the C_{phenyl}CNC_{pyridyl} torsion angles are of 179.14° and 168.48. Framework **3** is stabilized *via* hydrogen bonding interactions between the N_{amide} groups which strongly donate to the O_{amide} atoms [N1-H1N \cdots O3, D \cdots A 2.117(19) Å, <DHA 162°; N2-H2N \cdots O6, D \cdots A 2.6919(19) Å, <DHA 163°].



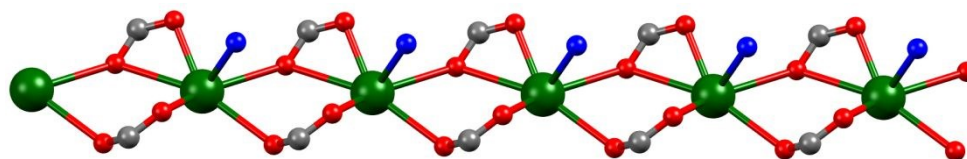
(a)



(b)



(c)

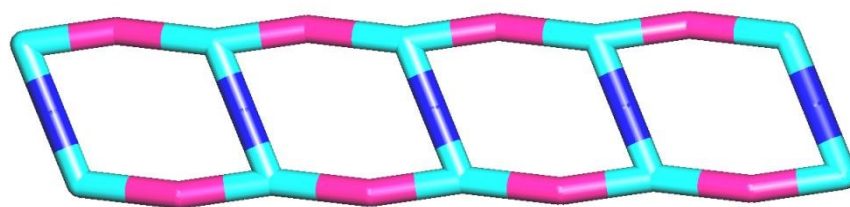


(d)

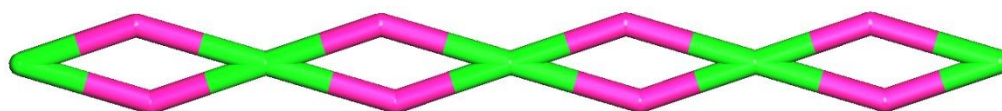
Fig. 3. (a) The molecular structure of **3** with partial atom labelling scheme, a fragment of its 2D network viewed down the crystallographic *b* (b) or *c* (c) axis, and (d) a chain of Pb(II)-bridging carboxylate groups which runs along the crystallographic *b* axis.

Topological Analysis of 1-3

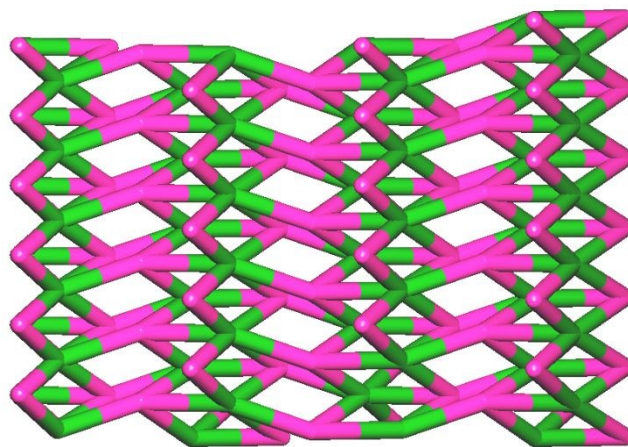
The topological analysis on CPs **1-3** was performed using TOPOS 4.0.17³⁶⁻³⁸ in order to comprehend the description of their crystal structures. CP **1** displays a 2,2,3-connected 3-nodal net with the point symbol $\{8^2.12\}_2\{8\}_3$ (Fig. 5a). The framework **2** has a 2,4-connected binodal net (Fig. 5b), but in the case of **3**, each Pb(II) is connected with seven different L⁻ ligands, one ligand connected to three Pb(II) centres and another ligand to four different metal centres. Thus, framework **3** represents a 3,4,7-connected trinodal net structure with topological type 3,4,7 (Fig. 5c).



(a)



(b)



(c)

Fig. 5. One dimensional double chain framework **1** (a) and **2** (b). The zinc and cadmium nodes are represented in cyan and green color, respectively. The linker is represented in pink colour and BDC is presented in blue. (c) Topological representation of framework **3** (Pb centres are in green colour and ligand in pink colour).

Thermogravimetric Analysis of 1-3

Thermogravimetric analyses (TGA) under dinitrogen in the range of 30-700 °C at a heating rate of 10 °C min⁻¹ were carried on CPs **1-3** in order to investigate their thermal stability. The TGA of **1** demonstrates a weight loss of 3.51 % (calculated = 3.75 %) at *ca.* 130-160 °C, accredited to the release of one coordinated water molecule followed by a weight loss of 13.93 % (calculated = 15.21 %) at 180-250 °C ascribed to the liberation of one non-coordinated DMF molecule. At *ca.* 250-380 °C the derived form was thermally stable, but above 380 °C the polymeric structure disintegrates leading to the formation of ZnO (Fig. 6). The TGA of **2** displays at 110-130 °C a weight loss of 5.91 % (calculated = 5.71 %) due to the release of one coordinated water molecule. The derived form was thermally stable up to 320 °C beyond which the polymeric structure

collapses and forms CdO (Fig. 6). On the other hand, CP **3** exhibits excellent thermal stability of up to *ca.* 400 °C, beyond which it disintegrates to form PbO (Fig. 6).

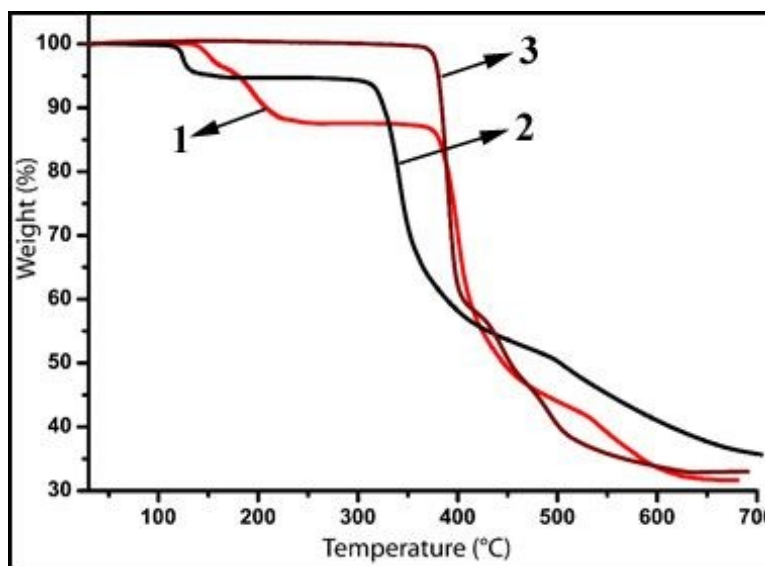


Figure 6: Thermogravimetric analysis of **1-3**.

Photoluminescent Properties of **1-3**

The luminescent properties of d^{10} metal complexes are well known and have marked their importance in numerous applications, namely in electroluminescence, chemical sensing, etc.^{39,40} Thus, in order to investigate the luminescent behaviour, the solid-state luminescent properties of the CPs **1-3** were studied at room temperature. Furthermore, the solid-state luminescent behaviour of the free pro-ligand **HL** was also inspected for comparison (Fig. 7). Upon excitation at $\lambda_{\text{ex}} = 290$ nm, **HL** exhibits an emission band at $\lambda_{\text{em}} = 415$ nm, which could be attributed to intra-ligand charge transfer transition.^{41,42} A higher emission peak with *ca.* 7 nm blue shift is observed for **1** at $\lambda_{\text{em}} = 408$ nm ($\lambda_{\text{ex}} = 320$ nm). The higher emission intensity observed for **1** could be due to intra-ligand transition of the coordinated L^- ; its coordination to the metal increasing its rigidity.^{41,42}

On the contrary, **2** exhibits photoluminescence of a similar nature to that of **HL** upon excitation at $\lambda_{\text{ex}} = 320$ nm, but with a decrease in emission intensity due to metal–ligand charge transfer transition.⁴³ A weaker photoluminescence was observed for **3** upon excitation at $\lambda_{\text{ex}} = 320$ nm.⁴³

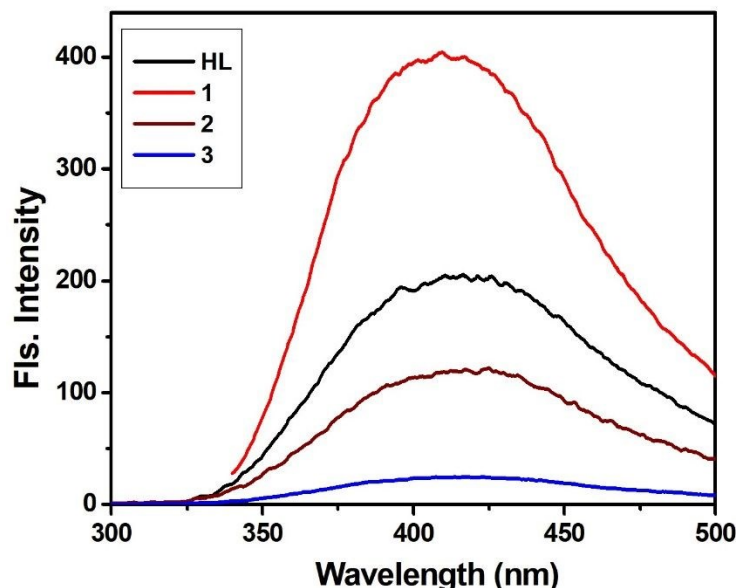


Fig. 7. Solid state emission spectra of **HL** and CPs **1-3** at room temperature.

Dye Adsorption Studies

Preliminary experimental results (Figs. S7 and S8 for **2** and **3**, respectively) demonstrated that **1** is the best compound for selective removal of an organic dye (discussed below). Thus, to appraise the ability of **1** for the removal of dyes from aqueous solution, four different kinds of dyes were chosen as model adsorbates, viz. Congo red (CR), rhodamine 6g (Rh-6g), rhodamine B (Rh-b) and fluorescein sodium (FI-Na), having different sizes and charges (Fig. 8). Experiments were typically carried out by immersing 10 mg of **1** in 3 mL of aqueous dye solution (3×10^{-5} M) in the dark at room temperature. The mixture was constantly stirred in the dark and the abilities of the sample to adsorb dyes from aqueous solution were monitored through UV-vis spectroscopy.

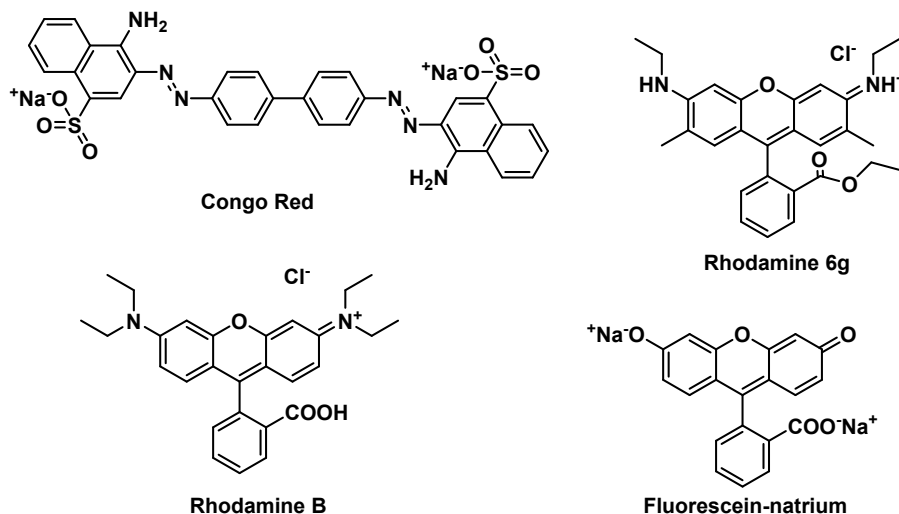


Fig. 8. Structure of Congo red (CR), rhodamine 6g (Rh-6g), rhodamine B (Rh-b) and fluorescein natrium (Fl-Na) used for dye separation studies.

The adsorption results of **1** towards the four organic dyes are depicted in Fig. 9. The naked eye visualization demonstrated a substantial adsorption of Congo Red (CR) dye in less than *ca.* 2 minutes, reaching completeness in only *ca.* 5 minutes. In contrast, no adsorption of Rh-6g, Rh-b or Fl-Na dyes were perceived even after more than 60 minutes of stirring at room temperature in the dark, what is also evidenced by UV-Vis spectroscopy (Fig. 10).

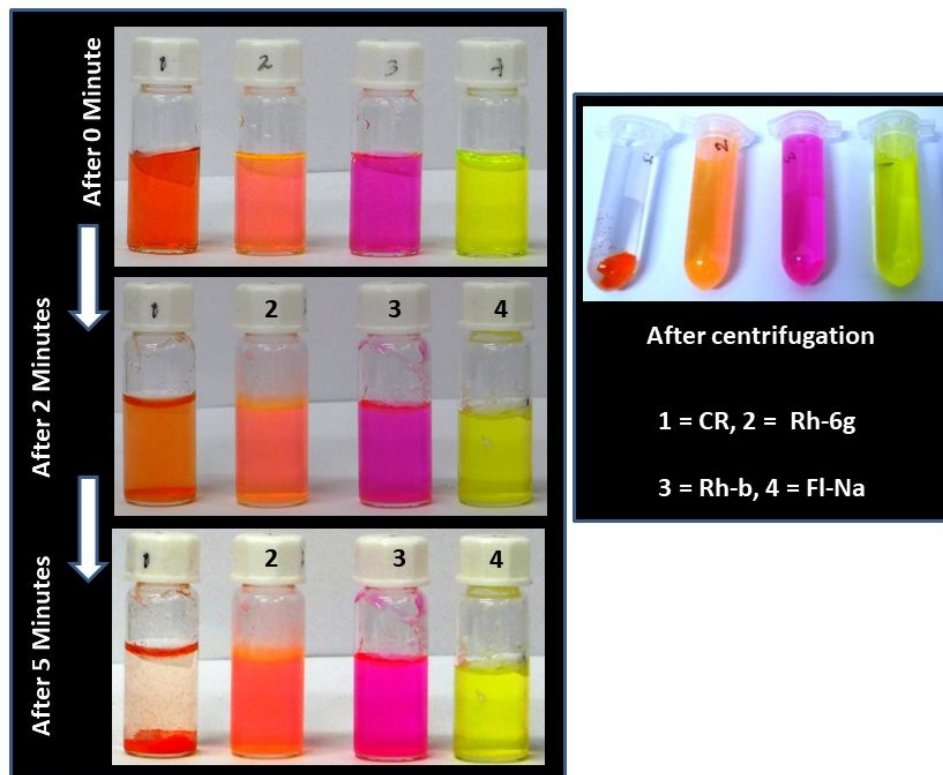


Fig. 9. Naked eye visualization on the removal of dyes by **1** at room temperature.

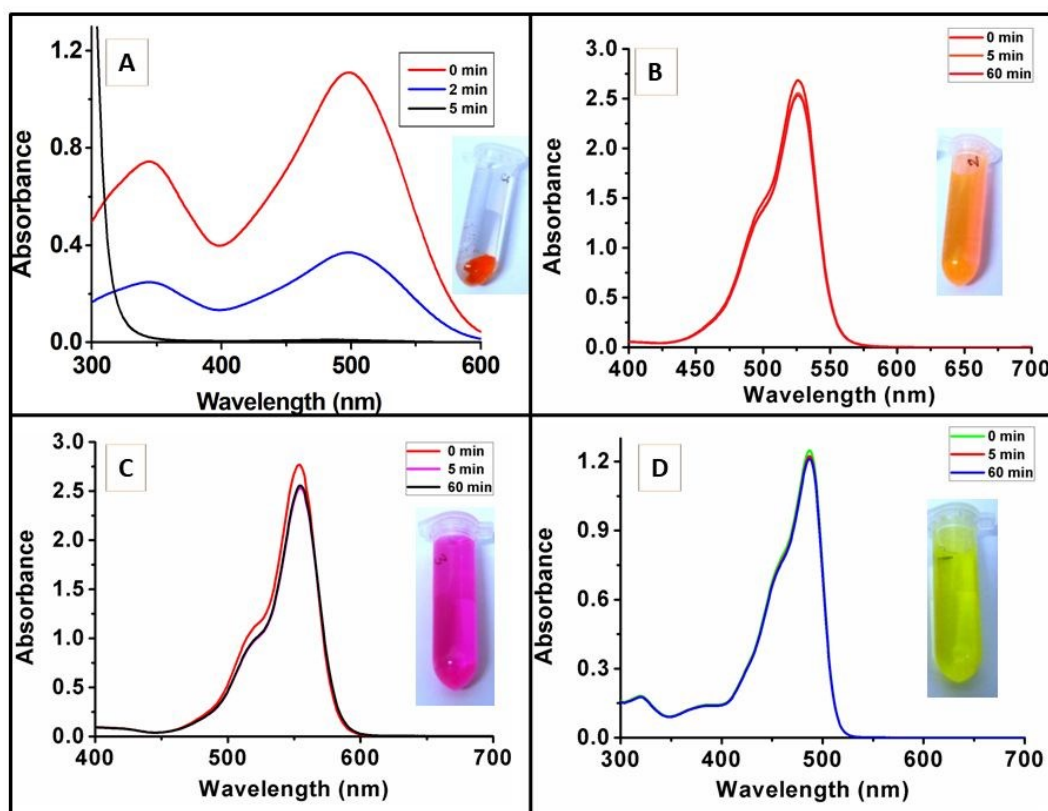


Fig. 10. UV-vis spectra of dye solutions upon adsorption on **1** at room temperature: (A) Congo red, (B) rhodamine 6g, (C) rhodamine B, and (D) fluorescein natrium.

The removal capacity of **1** (Removal%) was calculated using the following equation:

$$\text{Removal (\%)} = \frac{(A_o - A_t)100}{A_o}$$

where A_o and A_t represent the absorbance of the CR solution before and after the adsorption.

From the above equation, the CR removal capacity of **1** was found to be 99.54%, which is better than some of the reported CPs used for adsorption or removal of this dye.^{18,19,44,45} The adsorption property of **1** was also observed by its color change from transparent white (before adsorption) to reddish orange (after adsorption) (inset, Fig. S9, ESI). The structural integrity of **1** is

maintained throughout this adsorption process as supported by the scanning electron microscopy (SEM) images (Fig. S9, ESI) and EDX (Fig. S10, ESI) recorded before and after the adsorption of CR.

Furthermore, the point of zero charge (pHpzc)^{34,35} of the adsorbent 1 was determined to get an insight into its electronic and adsorption properties. The pHpzc is the pH where an adsorbent has zero total charge on its surface; above this point (higher pH) the surface is negatively charged, whereas below it (lower pH) the surface of the adsorbent is positively charged. The pHpzc of 1 was found to be 9.8 (Fig. S11, ESI) indicating that the surface has a net positive charge below pH 9.8 and a net negative charge above pH 9.8. CR is an anionic dye with a pKa of 5.5; when in solution, at pH lower than 5.5 it exists in cationic form presenting a blue color, while at higher pH it exists in anionic form with a red color.^{46,47} Thus, from our adsorption studies (see Fig. 9) at pH ca. 6.4, the effective removal of CR by 1 is consistent with the electrostatic attraction between the positively charged surface of 1 (pHpzc = 9.8) and the anionic CR in aqueous solution.

To understand if the selective adsorption of CR dye is determined by the presence of the azo (-N=N-) moiety in the framework and by the charge of the dye, the adsorption properties of 1 were investigated with related dyes bearing such a group, namely naphthol blue black (NBB) and orange II sodium salt (OR) (Fig. 11) by following a protocol similar to that mentioned above.

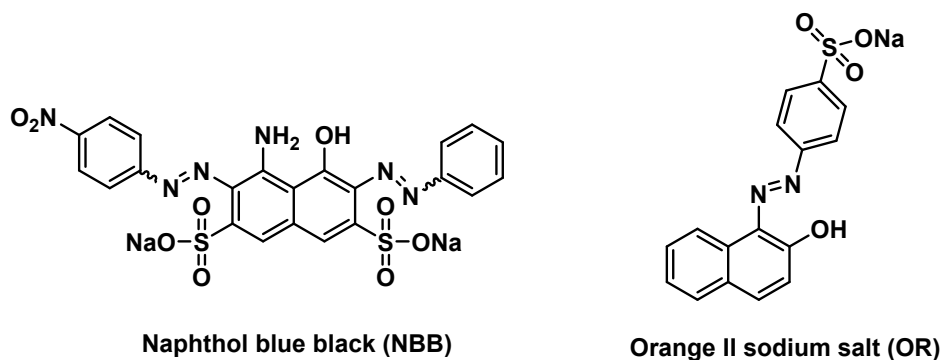


Fig. 11. Structure of Naphthol blue black (NBB) and Orange II sodium salt (OR).

The adsorption results of **1** towards these organic dyes are shown in Figs. 12 and 13, respectively. The naked eye visualization indicated that no or negligible adsorption of NBB dye in the first 5 minutes has occurred, although some adsorption was observed after ca. 60 minutes of stirring at room temperature in the dark as demonstrated by UV-Vis spectroscopy (Fig. 12). On the other hand, no adsorption of OR dye was seen even after ca. 60 minutes of stirring, what is also proved by UV-Vis spectroscopy (Fig. 13). These results clearly demonstrate the favorable selective adsorption of CR over other dyes even with a common azo moiety and also with a negative charge. Hence, such a selectivity is not primarily due to electrostatic attraction between the positively charged surface of **1** and the anionic CR, but is triggered by various noncovalent interactions including π - π stacking interactions with the framework of **1**, as shown by docking studies (see below, *in silico* docking studies).

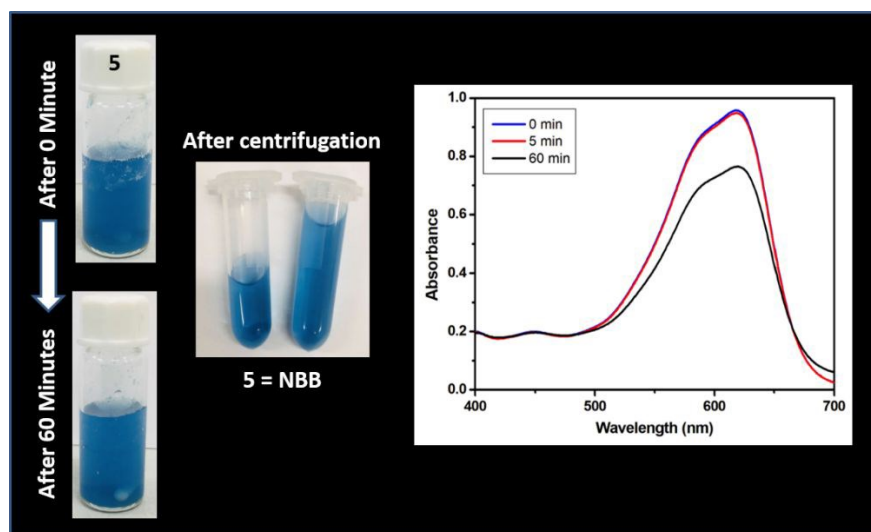


Fig. 12. Naked eye visualization on the removal of NBB dye by **1** at room temperature and its corresponding UV-vis spectrum.

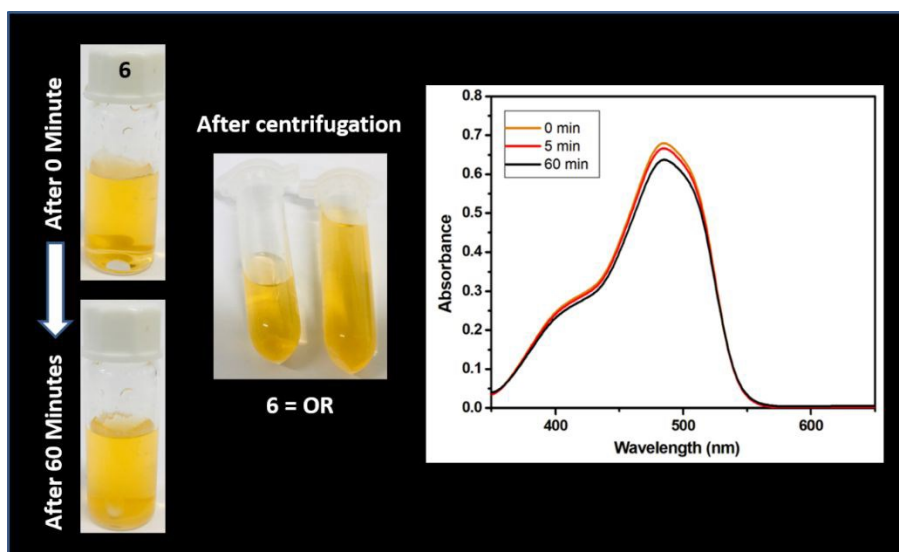


Fig. 13. Naked eye visualization on the removal of OR dye by **1** at room temperature and its corresponding UV-vis spectrum.

Selective Separation of CR dye

Compared to dye adsorption, dye selectivity is more attractive and challenging. This prompted us to investigate the selectivity of **1** towards the CR dye in mixed-dye solutions. The CR + Rh-6g, CR + Rh-b and CR + FI-Na dye mixtures were used. We have also tested the selectivity of **1** towards the CR dye in mixed-dye solutions containing CR + Rh-6g + Rh-b + FI-Na. As shown in Figs. 14 and 15, in each case only the CR could be selectively and efficiently adsorbed over a period of just 5 minutes. This fast and selective adsorption process of **1** is very important for adsorbents in practical wastewater treatment. As shown in the photographs (see inserted pictures in Figs. 14 and 15), after soaking **1** in the mixed-dye aqueous solutions, the solution color changed and finally retained the feature color of Rh-6g, Rh-b, FI-Na and Rh-6g + Rh-b + FI-Na, respectively. These results indicate that **1** can effectively and selectively adsorb CR molecules into the framework, from a solution containing a mixture of dyes.

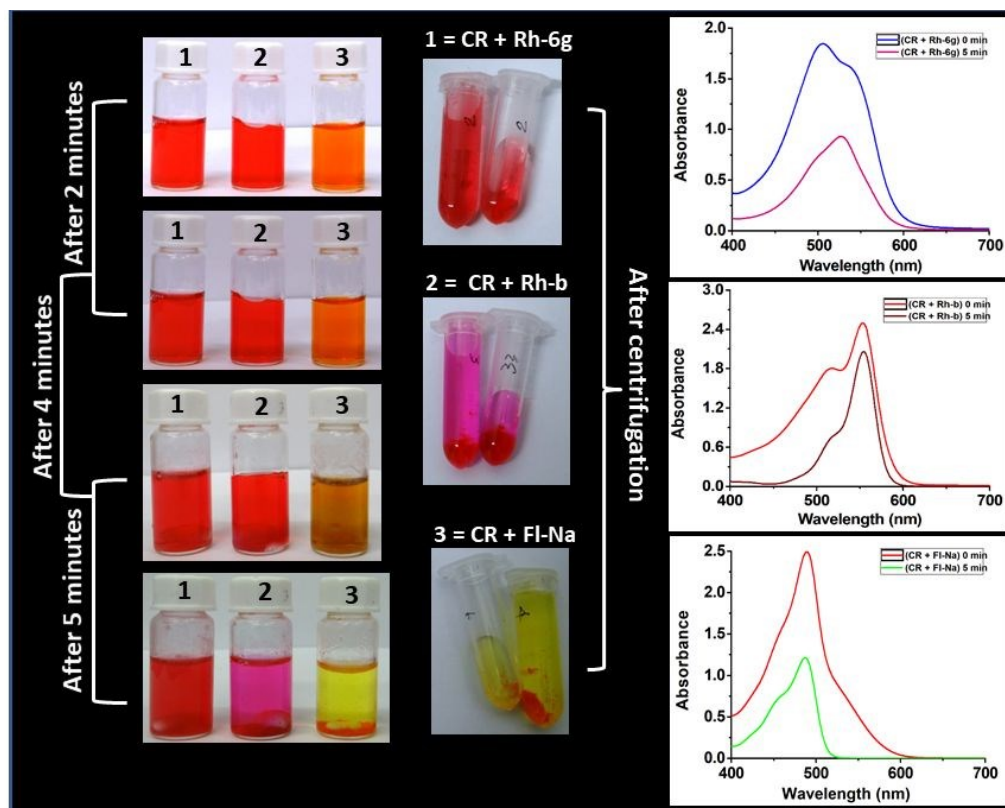


Fig. 14. Naked eye visualization of the adsorption of mixtures of dyes by **1** at room temperature and corresponding UV-vis spectra of the solutions.

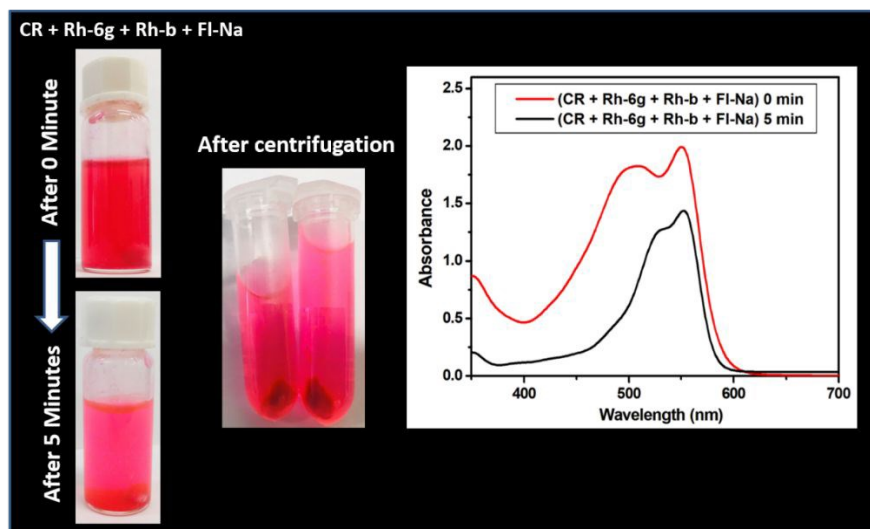


Fig. 15. Naked eye visualization of the adsorption of mixtures of dyes by **1** at room temperature and corresponding UV-vis spectra of the solutions.

Reusability of Adsorbent

To assess the reusability of the adsorbent, which contributes to reducing the cost of a practical application process, methanol, ethanol and acetonitrile were used in desorption and regeneration experiments, and methanol was found to have the best desorption effect. As soon as methanol was added to **1** with adsorbed CR (**1-CR**) the solution gained the CR colour almost instantaneously (Inset of Fig. 16). **1-CR** can expediently release the CR by simply washing the sample with methanol (for a 10 mg sample, ca. 1 mL methanol solvent was used). In addition, the dye removal capacity of **1** is fully maintained with recycling, its stability being evidenced by the IR spectrum of **1** (Fig. S12, ESI) recorded after each cycle. As depicted in Fig. 16, after recycling three times, **1** showed almost identically rapid and quantitative adsorption of CR. Accordingly, **1** is an excellent candidate as a selective adsorption material, which eventually can be applied practically to adsorb CR in mixed-dye containing wastewater. This strong and selective adsorption of CR by **1** can be accounted for by different types of interactions as discussed below.

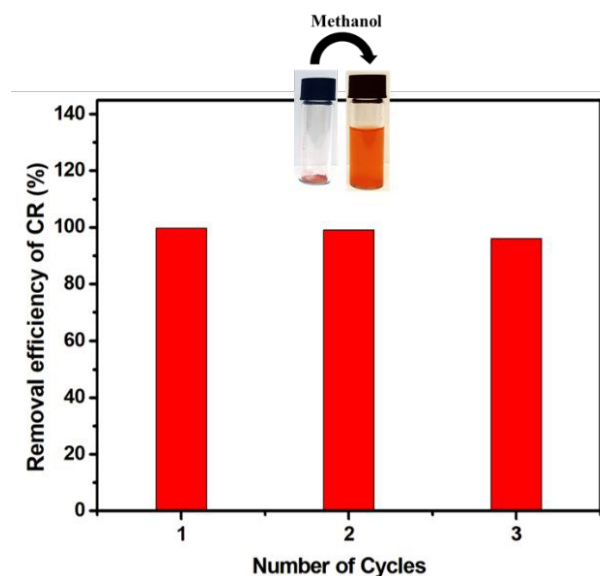


Fig. 16. Effect of CP 1 recycling on the adsorption of CR.

In Silico Studies

We carried out docking studies in order to get a visual representation and insight into the selective adsorption of CR on **1** (Fig. 17). The full geometry optimization of Congo Red (CR), rhodamine 6g (Rh-6g), rhodamine B (Rh-b) and fluorescein sodium (Fl-Na) has been carried out using ChemDraw 3d software. The type of interaction taking place between **1** and CR was studied by adopting molecular docking software using HEX 8.0.0 software and visualization was performed using Discovery Studio 3.5 software.

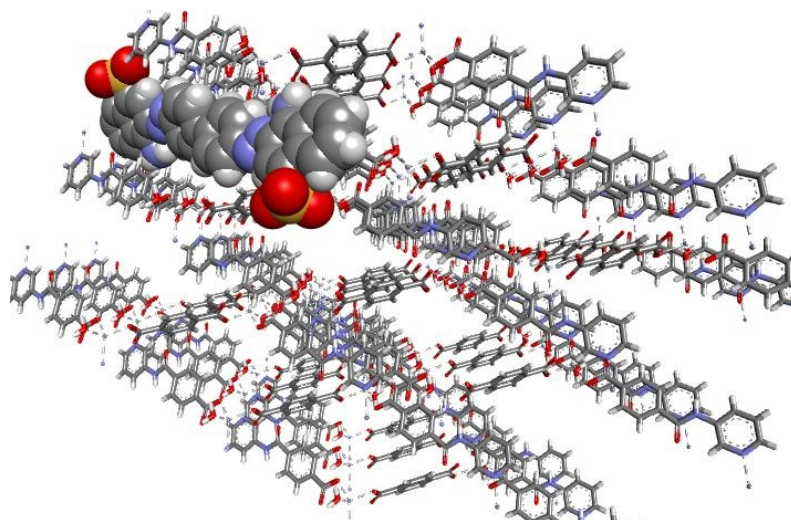


Fig. 17. Visualization of the docked CR in **1**.

The docking study reveals that the dyes stick to the 1D polymer of **1**, with a relative binding energy of -443.75 (CR), -301.45 (Rh-6g), -304.83 (Rh-b) and -231.70 (FI-Na) eV. The results unambiguously support the stronger binding affinity of CR, which is in harmony with the spectroscopic studies. The stacking of CR in **1** is depicted in Fig. 18 and shows the interactions that are responsible for the adsorption process, specifically anion- π , cation- π and π - π stacking interactions (Fig. 18). The phenyl rings of L^- and the phenyl and naphthalene rings of CR are involved in the π - π stacking interactions, which are in the range of 3.84-4.13 Å. The anion- π interactions connect not only the CR $O_{\text{sulfonate}}$ with the phenyl ring of L^- , but also the $O_{\text{carboxylate}}$ of L^- and the CR phenyl ring with distances of 4.28 Å and 4.77 Å, respectively. A strong cation- π interaction with a distance of 3.58 Å is disclosed between Zn(II) ion and a naphthalene ring. These interactions are thought to be the main driving force for the selective adsorption or removal ability of CR by **1**, that are favored by the elongated shape of the CR dye and by the structural widening of **1** due to the BDC spacer which can facilitate *e.g.* a strong π - π staking with the ligand framework of **1** leading to an effective adsorption.

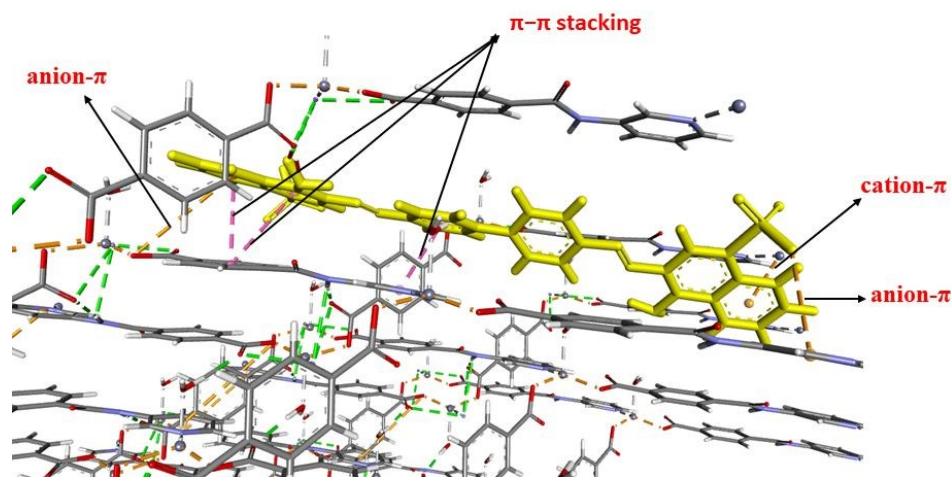


Fig. 18. The intermolecular interactions responsible for the stacking of CR in **1**.

Surface Area and Porosity Measurement using nitrogen adsorption-desorption isotherm

The dye capture in solution encourages to measure the surface area and porosity of the synthesized CPs **1-3**. N₂ adsorption isotherms based on the Brunauer–Emmett–Teller (BET) adsorption/desorption model were studied at 77 K [Fig. 19(a)].^{48,49} CPs **1-3** exhibited type II isotherms, with BET surface areas of 31.9, 6.4 and 5.8 m²/g, respectively, with *H3* hysteresis suggesting non-rigid absorbent. DFT pore size distribution (PSD) [Fig. 19(b)] revealed a higher total volume in pores for **1** (0.063 cm³/g) relative to **2** or **3** (0.020 or 0.010 cm³/g) with pores in both the micropore (between 1.0 and 1.3 nm) and mesopore region (above 2 nm). The higher BET surface area obtained for **1** was expected in view of the potential void measured by X-ray diffraction (see above) and is due to the structural effect of its benzene-1,4-dicarboxylate (BDC) linker which originates an open structure.⁵⁰

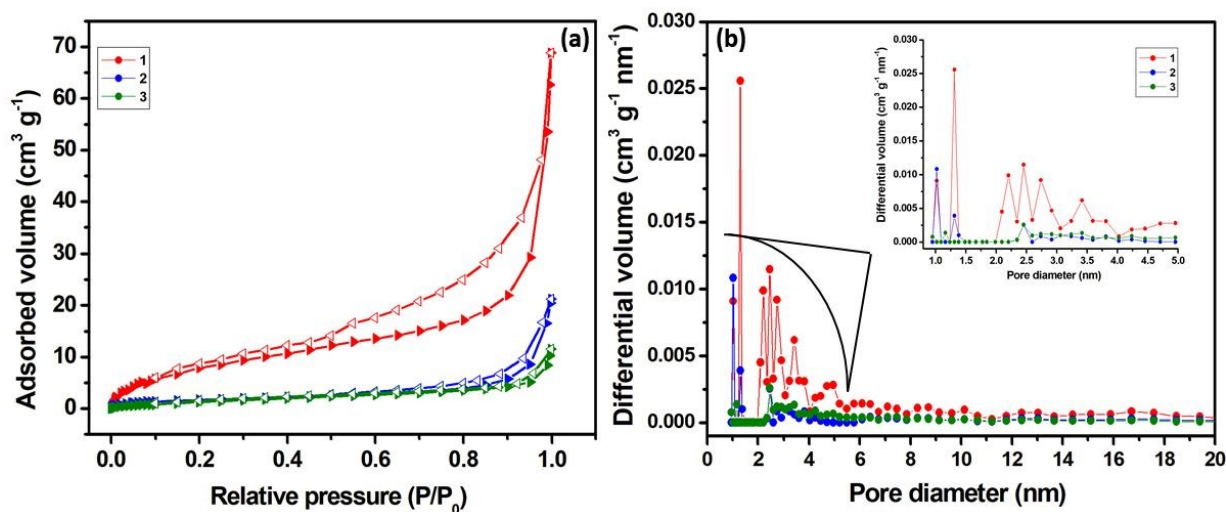


Fig. 19. N₂ adsorption isotherms at 77 K (the empty symbols indicate the desorption branches) for **1-3** (a) and DFT pore size distribution (b).

The results indicate that despite the difference in the surface area of **1** relative to those of **2** and **3**, they have similar pore sizes. The observed selectivity of CR adsorption by **1** should be mainly driven by the various kinds of interactions as supported by *in silico* studies.

Conclusion

We have synthesised and characterized three new coordination polymers of Zn(II), Cd(II) and Pb(II) (CPs **1-3**, respectively) using 4-(pyridin-3-ylcarbamoyl)benzoic acid (**HL**) as ligand source. The single-crystal X-ray diffraction analysis disclose their polymeric character. CP **1** exhibits a selective adsorption/removal of Congo Red (CR) dye among various tested dyes; it can be recycled and reused for several times without a significant loss of its dye removal efficiency. This selective removal of CR by **1** is accounted for by various noncovalent interactions, such as anion- π , cation- π and π - π stacking interactions with the framework of **1** as substantiated by *in silico* studies (docking). The adsorption is also favoured by electrostatic interactions between the positively charged surface of adsorbent and the negatively charged surface of the dye in aqueous solution. The higher surface area of **1** in comparison with those of **2** and **3** can favour a higher adsorption ability of the former, but the selectivity towards CR cannot be explained on the basis of the pore size.

ACKNOWLEDGEMENTS

This work has been partially supported by the Fundação para a Ciência e a Tecnologia (FCT), Portugal, through projects UIDB/00100/2020 of Centro de Química Estrutural. The authors A.P.

and A.K. are grateful to the FCT and IST, Portugal, for financial support through "DL/57/2017" (Contract no. IST-ID/197/2019 and IST-ID/107/2018). The authors also acknowledge the Portuguese NMR Network (IST-UL Centre) for access to the NMR facility and to the IST Node of the Portuguese Network of Mass-spectrometry for ESI-MS measurements.

Supporting Information

Electronic Supplementary Information (ESI) available: Figures S1-S12 containing FTIR, ^1H , ^{13}C - NMR, PXRD, SEM, EDX, UV-vis and pH measurement. Selected bond distances and angles are presented in Table S1-S2. CCDC 2010625-2010627.

References

- 1 F. M. Drumond Chequer, G. A. R. de Oliveira, E. R. Anastacio Ferraz, J. Carvalho, M. V. Boldrin Zanoni and D. P. de Oliveir, *Eco-Friendly Text. Dye. Finish. InTech IntechOpen*;
- 2 Y. Bayrak and R. Uzgor, *Asian J. Chem.*, 2013, **25**, 71–78.
- 3 J. X. Li, Z. C. Hao, L. Ren and G. H. Cui, *Zeitschrift fur Anorg. und Allg. Chemie*, 2018, **644**, 1196–1202.
- 4 H. Zhu, D. Liu, Y. H. Li and G. H. Cui, *Polyhedron*, 2019, **167**, 44–50.
- 5 Y. Wang, X. Dai, Y. Zhan, X. Ding, M. Wang and X. Wang, *Int. J. Biol. Macromol.*, 2019, **137**, 77–86.
- 6 D. D. Guo, B. Li, Z. P. Deng, L. H. Huo and S. Gao, *Ecotoxicol. Environ. Saf.*, 2019, **178**, 221–229.
- 7 C. Li, Z. Xiong, J. Zhang and C. Wu, *J. Chem. Eng. Data*, 2015, **60**, 3414–3422.
- 8 Y. P. Wu, X. Q. Wu, J. F. Wang, J. Zhao, W. W. Dong, D. S. Li and Q. C. Zhang, *Cryst. Growth Des.*, 2016, **16**, 2309–2316.
- 9 J. R. Li, J. Sculley and H. C. Zhou, *Chem. Rev.*, 2012, **112**, 869–932.
- 10 H. Kaur, S. Sundriyal, V. Pachauri, S. Ingebrandt, K. H. Kim, A. L. Sharma and A. Deep, *Coord. Chem. Rev.*, 2019, **401**, 213077–213098.
- 11 H. ŌKawa, Y. Yoshida, K. Otsubo and H. Kitagawa, *Inorg. Chem.*, 2020, **59**, 26.
- 12 M. Kurmoo, *Chem. Soc. Rev.*, 2009, **38**, 1353–1379.
- 13 A. Paul, A. Karmakar, M. Fátima, C. Guedes Da Silva and A. J. L. Pombeiro, *RSC Adv.*, 2015, **5**, 87400–87410.

- 14 A. Paul, A. P. C. Ribeiro, A. Karmakar, M. F. C. Guedes da Silva and A. J. L. Pombeiro, *Dalt. Trans.*, 2016, **45**, 12779–12789.
- 15 A. Karmakar, A. Paul, K. T. Mahmudov, M. F. C. Guedes Da Silva and A. J. L. Pombeiro, *New J. Chem.*, 2016, **40**, 1535–1546.
- 16 A. Karmakar and A. J. L. Pombeiro, *Coord. Chem. Rev.*, 2019, **395**, 86–129.
- 17 S. W. Lv, J. M. Liu, Z. H. Wang, H. Ma, C. Y. Li, N. Zhao and S. Wang, *J. Environ. Sci. (China)*, 2019, **80**, 169–185.
- 18 F. L. Hu, Y. X. Shi, H. H. Chen and J. P. Lang, *Dalt. Trans.*, 2015, **44**, 18795–18803.
- 19 M. Y. Masoomi, A. Morsali and P. C. Junk, *CrystEngComm*, 2015, **17**, 686–692.
- 20 H. N. Wang, F. H. Liu, X. L. Wang, K. Z. Shao and Z. M. Su, *J. Mater. Chem. A*, 2013, **1**, 13060–13063.
- 21 J. Duan, J. Bai, B. Zheng, Y. Li and W. Ren, *Chem. Commun.*, 2011, **47**, 2556–2558.
- 22 O. Benson, I. Da Silva, S. P. Argent, R. Cabot, M. Savage, H. G. W. Godfrey, Y. Yan, S. F. Parker, P. Manuel, M. J. Lennox, T. Mitra, T. L. Easun, W. Lewis, A. J. Blake, E. Besley, S. Yang and M. Schröder, *J. Am. Chem. Soc.*, 2016, **138**, 14828–14831.
- 23 J. Lin, Q. Cheng, J. Zhou, X. Lin, R. C. K. Reddy, T. Yang and G. Zhang, *J. Solid State Chem.*, 2019, **270**, 339–345.
- 24 Z. Tang, H. Chen, Y. Zhang, B. Zheng, S. Zhang and P. Cheng, *Cryst. Growth Des.*, 2019, **19**, 1172–1182.
- 25 S. K. Konavarapu, A. Goswami, A. G. Kumar, S. Banerjee and K. Biradha, *Inorg. Chem. Front.*, 2019, **6**, 184–191.
- 26 A. Paul, L. M. D. R. S. Martins, A. Karmakar, M. L. Kuznetsov, A. S. Novikov, M. F. C. Guedes da Silva and A. J. L. Pombeiro, *J. Catal.*, 2020, **385**, 324–337.
- 27 W. Y. Xu, X. Z. Tian, X. F. Feng, H. X. Huang, G. M. Sun, Y. M. Song and F. Luo, *CrystEngComm*, 2012, **14**, 8418–8423.
- 28 A. Paul, L. M. D. R. S. Martins, A. Karmakar, M. L. Kuznetsov, M. F. C. Guedes da Silva and A. J. L. Pombeiro, *Molecules*, 2020, **25**, 2644.
- 29 W. L. F. A. and D. R. P. D. D. Perrin, *Purif. Lab. Chem. Pergamon Oxford, U.K. 1986.*
- 30 *Bruker, APEX2. Bruker AXS Inc., Madison, Wisconsin, USA, 2012.*
- 31 G. M. Sheldrick, *SADABS. Progr. Empir. Absorpt. Correct. Univ. Gottingen, Ger. 2000.*
- 32 G. M. Sheldrick, *Acta Crystallogr.*, 2015, **C71**, 3–8.
- 33 L. J. Farrugia, *J. Appl. Crystallogr.*, 2012, **45**, 849–854.
- 34 N. Fiol and I. Villaescusa, *Environ. Chem. Lett.*, 2009, **7**, 79–84.
- 35 M. N. Khan and A. Sarwar, *Surf. Rev. Lett.*, 2007, **14**, 461–469.
- 36 M. O. and O. M. Yaghi, *Reticular Chem. Struct. Resour. Arizona State Univ. Tempe, AZ, 2005, [Http://rcsr.anu.edu.au/](http://rcsr.anu.edu.au/).*
- 37 V. A. Blatov, *IUCr, Comput. Comm. Newslett.*, 2006, **7**, 4, <http://www.topos.ssu.samara>.

- 38 V. A. Blatov, *Struct. Chem.*, 2012, **23**, 955–963.
- 39 S. Pramanik, C. Zheng, X. Zhang, T. J. Emge and J. Li, *J. Am. Chem. Soc.*, 2011, **133**, 4153–4155.
- 40 A. Lan, K. Li, H. Wu, D. H. Olson, T. J. Emge, W. Ki, M. Hong and J. Li, *Angew. Chemie - Int. Ed.*, 2009, **48**, 2334–2338.
- 41 W. Q. Kan, B. Liu, J. Yang, Y. Y. Liu and J. F. Ma, *Cryst. Growth Des.*, 2012, **12**, 2288–2298.
- 42 P. Cui, J. Wu, X. Zhao, D. Sun, L. Zhang, J. Guo and D. Sun, *Cryst. Growth Des.*, 2011, **11**, 5182–5187.
- 43 Y. J. Cho, S. Y. Kim, H. J. Son, D. W. Cho and S. O. Kang, *Phys. Chem. Chem. Phys.*, 2017, **19**, 8778–8786.
- 44 B. Wu, W. H. Zhang, Z. G. Ren and J. P. Lang, *Chem. Commun.*, 2015, **51**, 14893–14896.
- 45 L. N. Jin, X. Y. Qian, J. G. Wang, H. Aslan and M. Dong, *J. Colloid Interface Sci.*, 2015, **453**, 270–275.
- 46 X. Guo, L. Kong, Y. Ruan, Z. Diao, K. Shih, M. Su, L. Hou and D. Chen, *J. Colloid Interface Sci.*, 2020, **578**, 500–509.
- 47 M. Chahkandi, *Mater. Chem. Phys.*, 2017, **202**, 340–351.
- 48 F. Ambroz, T. J. Macdonald, V. Martis and I. P. Parkin, *Small Methods*, 2018, **2**, 1800173.
- 49 N. Mosca, R. Vismara, J. A. Fernandes, S. Casassa, K. V. Domasevitch, E. Bailón-García, F. J. Maldonado-Hódar, C. Pettinari and S. Galli, *Cryst. Growth Des.*, 2017, **17**, 3854–3867.
- 50 J. D. Humby, O. Benson, G. L. Smith, S. P. Argent, I. Da Silva, Y. Cheng, S. Rudić, P. Manuel, M. D. Frogley, G. Cinque, L. K. Saunders, I. J. Vitorica-Yrezábal, G. F. S. Whitehead, T. L. Easun, W. Lewis, A. J. Blake, A. J. Ramirez-Cuesta, S. Yang and M. Schröder, *Chem. Sci.*, 2019, **10**, 1098–1106.

Table 1: Crystal data and structure refinement details for compounds **1-3**.

	1	2	3
Empirical formula	C ₂₀ H ₂₀ N ₃ O ₇ Zn	C ₂₆ H ₂₂ CdN ₄ O ₈	C ₂₆ H ₁₈ N ₄ O ₆ Pb
Formula weight	479.76	630.87	689.63
Crystal system	triclinic	triclinic	monoclinic
Space group	P-1	P-1	P2 ₁ /n
Temperature (K)	298(2)	296(2)	296(2)
<i>a</i> (Å)	8.554(3)	7.7745(5)	17.1194(13)
<i>b</i> (Å)	11.089(4)	8.7385(6)	5.1144(3)
<i>c</i> (Å)	11.895(4)	10.6928(7)	25.2616(15)
<i>α</i> (°)	90.098(9)	105.022(2)	90

β (°)	110.130(12)	95.322(3)	92.795(4)
γ (°)	90.113(9)	116.297(2)	90
V (Å ³)	1059.4(6)	610.66(7)	2209.2(2)
Z	2	1	4
D_{calc} (g/cm ³)	1.504	1.716	2.073
μ (mm ⁻¹)	1.206	0.955	7.692
F000	494	318	1328
Refl. collected	30647	6142	49021
Refl. obs / unique	4332 / 3775	2200 / 2187	4546 /
N° of parameters	290	187	340
R _{int}	0.0261	0.0106	0.0323
$R(F)$ ($I \geq 2\sigma$)	0.0599	0.0167	0.0199
$wR(F^2)$ (all data)	0.1298	0.0444	0.0438
GOF (F^2)	1.130	1.109	1.069

Graphical abstract

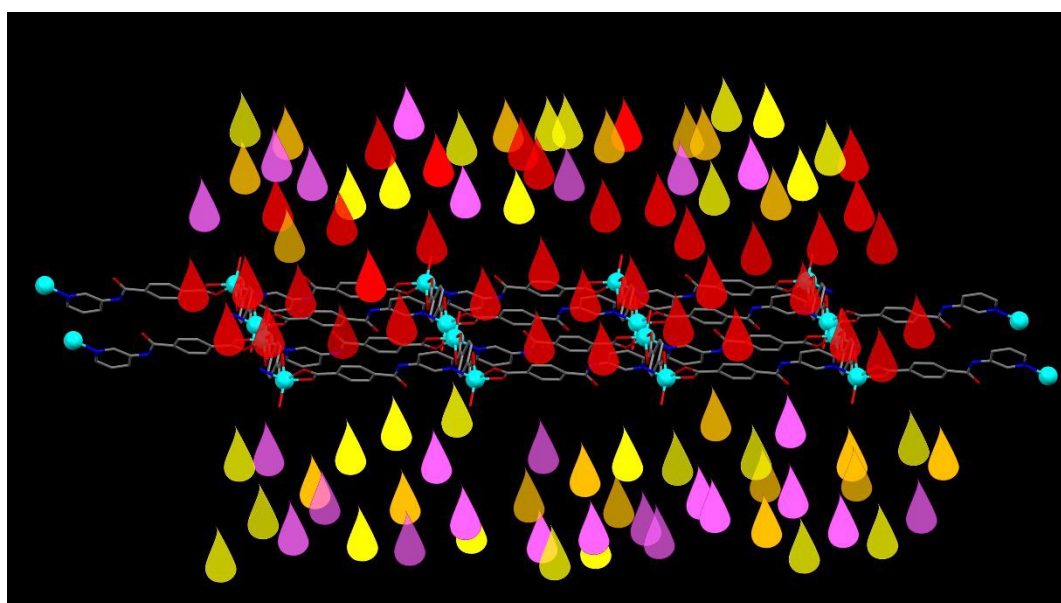
View Article Online
DOI: 10.1039/D0DT02172E

A mechanistic insight into the rapid and selective removal of Congo Red by an amide functionalised Zn(II) Metal Organic Framework

Anup Paul,^{*,†} Kabita Das,[‡] Anirban Karmakar,[†] M. Fátima C. Guedes da Silva, Armando J. L. Pombeiro^{*,†}

[†]*Centro de Química Estrutura, Instituto Superior Técnico, Universidade de Lisboa, Av. Rovisco Pais, 1049-001 Lisboa. Portugal.*

[‡]*Department of Environmental Studies, North-Eastern Hill University, Meghalaya, Shillong 793022, India*



1D Zn(II) CP **1** exhibits a selective removal of Congo Red dye amongst various dyes.